International Society for Rock Mechanics and Rock Engineering
Norwegian Group for Rock Mechanics

ISRM International Symposium
Eurock 2025 – Expanding the Underground Space
Trondheim, Norway, 16-20 June
ISBN 978-82-8208-079-8

Prediction of residual rockfall risk in presence of net fences according to the position of the impact

V. De Biagi, M. Marchelli & F. Pimpinella
Politecnico di Torino, Torino, Italy
valerio.debiagi@polito.it

Abstract

Residual risk assessment in presence of structural mitigation measures represents a challenging issue as the risk in a given time framework, e.g. the annual risk, should be quantified. This presupposes the knowledge of the frequency-magnitude relationship of the considered geohazard. To lower the risk below an acceptable threshold, protective measures are often installed. Structural systems have an inherent failure probability that should be accounted in the computation of the residual risk.

Dealing with rockfall hazard, the present work proposes an enhanced version of a reliability-based approach to quantify the failure probability of net fences and the residual risk. Net fences are complex systems, made by assembling several metallic components with different functions. For each system, the performance is certified by standards tests that presuppose that the impact occurs in the center of the fence. Previous works by the authors considered the capacity of the barrier being distributed with a Dirac-delta function at the certified energy absorption capacity. Anyway, the energy absorption capacity of a net fence varies according to impact position and impacting features.

This paper proposes a new distribution of the resisting capacity of the barrier based on the different position of the impact thanks to a numerical FEM investigation on a real barrier. An example of application is included. The proposed method thus allows predicting the risk reduction in presence of net fences, accounting for the possible rock impacts. The procedure can provide the basics to be tailored for other geohazards or different structural protective measures.

Keywords

Rockfall barrier, reliability analysis, numerical model

1 Introduction

In mountainous regions, inhabited areas and infrastructure may be seriously threatened by rockfall, a high energy natural hazard. To lower the risk of rockfall, one of the most popular passive structural systems is the rockfall net fence (also known as rockfall flexible barrier). Installed along the slope where the natural event is anticipated, this device can intercept the blocks and slow their movement up to the complete rest because it dissipates energy through the structural system's permanent deformation. A rockfall barrier comprises three main components: an interception structure, a support structure, and connection components. The interception structure, i.e. a net made of metallic ropes or wires, may include a finer mesh for small rock pieces. It deforms elastically and plastically, transferring impact forces to the connection components. The support structure, consisting of metallic posts hinged to base plates, maintains the interception structure's position. Connection components,

such as ropes and wire rope clips, transfer impact forces to the foundations. Energy dissipating devices, which dissipate energy through deformation or friction, are often integrated into the ropes (Pimpinella et al., 2024). This systemis an industrial product that can be bought as a kit, characterized by its energy absorption capacity of the system, namely the MEL, and height. The MEL is determined through specific tests performed, in Europe, according to EAD 340059-00-0106 (EOTA, 2018).

For the tests, three functional modules, i.e. a system with 4 posts, are considered: two lateral and one central. The MEL is experimentally assessed by an impact of a predefined kinetic energy in the center of the central module, i.e. in controlled conditions, only. A specific block shape and mass is defined as well. As a consequence, the resistance of the system, expressed in terms of energy absoption capacity E_b, can be represented by a Dirac-δ distribution on the MEL value. The test does not represent all the possible impact scenarios that can occur, neither in terms of block volumes nor impact locations. Consequently, the measure of their effectiveness in a risk mitigation and management process represents a difficult task.

Moreover, to assess the residual risk where protective measures as net fences have been installed, it is crucial to know their failure probability in a given time period, as they are susceptible to failure like any other technical system exposed to hazards. Recently, the authors included the failure probability of the protective structures into the quantification of the risk in a mountain site without or with rockfall barriers (Marchelli et al. 2024).

The hazard assessment requires knowledge of the distribution of all possible block masses that can detach, along with their temporal detachment probability. Studies indicate that smaller rock volumes are more prone to detachment than larger blocks. Research on in-situ block size distributions suggests that rock mass discontinuities identify potentially unstable blocks, with volumes following an exponential-like distribution (Moos et al., 2022). Rockfall propagation is influenced by various variables, resulting in site-dependent distributions of possible impacted energies and masses. To quantify the risk, i.e., the possible effects on the elements at risk, the vulnerability of such elements should be analyzed for all possible impacting scenarios, considering their resisting capabilities. A similar approach should be applied to protective structures.To compute the failure probability of the barrier, the Authors have formulated a mathematical framework that is based on reliability-based approaches, as required by the modern design techniques (De Biagi et al. 2020; Marchelli et al. 2020, 2021). The method allows for considering of all possible block volumes that can reach the mitigation measure, in contrast to other approaches found in the literature or in the standards, e. g. the UNI 11211-4 (2018). In this last, the design is done starting from single values (i.e. the characteristic values) of the mass, velocity, trajectory height of the design block, and barrier capacity (UNI, 2018). Although the details of the procedure proposed by the Authors can be found in the reference literature, in a simplified formulation, the barrier failure probability F_k when the block kinetic energy exceeds the barrier capacity, within a number *t* of years is:

$$F_k = 1 - \exp\left[-\lambda t \int_0^{\infty} p_f(\mu) f_{m_k}(\mu) d\mu\right] \quad (1)$$

Where λ Average frequency of rockfall events along the slope
$f_{m_k}(\mu)$ Probability that the fallen block has mass equal to μ
$p_f(\mu)$ Probability that the state function $K = E_b - \frac{1}{2}mv^2$ has negative values if the falling block has mass equal to μ.

The relevant points of the approach are the fact that the probabilities are integrated over all potential volumes and that the p_f is obtained from an integration of probabilities. Details on how obtaining the average frequency and impacting volumes probability distributions are provided in the references (De Biagi et al. 2020; Marchelli et al., 2020, 2021). While very precise in determining the actions, the method, in its present form, lacks information to quantify the resistance of the barrier for different scenarios. A similar approach is adopted to asses the failure due to excessive trajectories heights compared to the height of the product. As mentioned before, a barrier is placed on the marked providing the MEL value, only. To obtain a more reiliable quantification of the performance of the barrier, the present study investigates the effects of non-centered impacts. This is the first step to implement a probability density for the capacity E_b that considers the real impact conditions. The same shape and volume used in standardized tests are adopted to make results comparable with field tests

and to provide suggestions for possible further impact tests to be replicated by producers. The combined effects of different volumes, shapes and impact locations will be assessed in the future. Knowing the trajectory of the blocks, the results can have an impact also in the design of the more suitable height to be required by the protective measures, as well in the choice of the starting and ending position of the barrier. The analysis is carried on through a finite element (FE) model of a 1000 kJ barrier made by Geobrugg, as detailed in the following.

2 FE model of Geobrugg RXI-100 rockfall barrier

RXI-100 from Geobrugg AG is a rockfall barrier system which has been widely used in the first decade of the current century, with a MEL of 1000 kJ. The model was created in Abaqus CAE software framework (v.2024) and calibrated thanks to the Swiss approval certificate and internal test reports from Geobrubb AG. In the former, braking time, i.e. the time required to stop the impacting mass, and braking distance at MEL conditions are declared, together with maximum forces on wire rope cables and brakes elongations. Fig. 1 reports a general view of the model. In RXI-100, the intercepting structure is constituted by a four contact points wire ring net R12/3/300 (windings/wire diameter/ring diameter, in mm). Wire rings steel nets have been exstensively tested with quasi-static punching tests (Xu et al. 2018) and numerous numerical simulations have been developed modelling the intercepting structure with an equivalent shell element with limited errors (Jin et al. 2021). Similarly, an equivalent membrane approach is adopted in our model and the costitutive parameters of the membrane are taken from Jin et al. (2021). The behaviour of the net is substantially plastic, but a reduced elastic phase is considered. This enables the simulation of the rebound phase, which follows the attainment of maximum elongation in the structure.

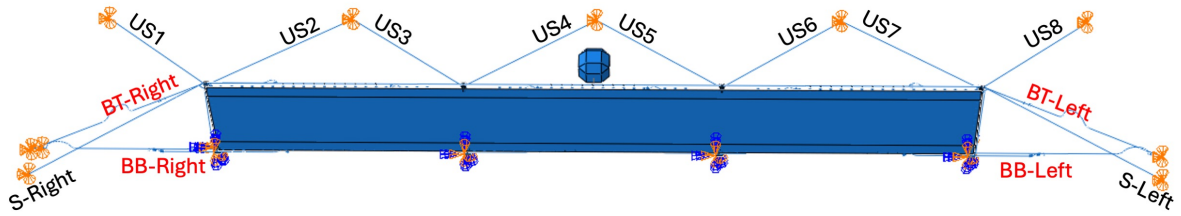

Fig. 1 General view of the FE model with indication of the ropes further recalled in the paper. Right and left are defined from an upslope reference system.

In the present barrier, a 6x19 class wire rope cables were considered. The pseudo-elastic behaviour of wire ropes appears after an initial phase in which the steel wires mainly slide along each other, producing an initial elongation with a low stressing force value. This aspect was considered in our model by introducing an artificial loop within all the sustaining and longitudinal ropes, with an approach similar to the one proposed in Escallón et al. (2014). Whenever coupled ropes are foreseen in the barrier installation scheme, single ropes with an equivalent diameter were introduced in the model. In the RXI-100 system, energy dissipators are mounted on the longitudinal ropes, only, with a total of 16 GS-8002 brake rings (Qi et al. 2018). Specifically, two brake rings are installed in series on each longitudinal rope at both sides near the foundations. In our model, four brake elements were used, each representing the behavior of four brake rings in the real system. This approach aligns with the experimental findings of Qi et al. (2018), which demonstrate that the mechanical behavior of brake rings arranged in series or parallel closely resembles that of single rings. The braking elements were added to the model by introducing an artificial separation within the longitudinal cables near the anchor points and filling the resulting gap with an axial connector. The associated force-displacement behaviour was obtained by scaling the behaviour of the single rings on both axis. Steel posts were modelled with shell elements with a Cowper-Symonds power hardening law and a Johnson-Cook damage model to account for impacts on posts and adopted S355 steel parameters as found in literature (Forni et al. 2016, Ribeiro et al. 2016). The post was connected to the ground plate via a shell element tied to the web of the post profile, simulating bolting and welding on one side, while several connecting components were included to replicate a one-directional hinge. The connection between the sustaining ropes and the steel post was modeled by accurately reproducing the shape of the post head and positioning the steel ropes within the assembly. All the connections between the

steel posts and wire rope cables were made by introducing restraints tied to the steel posts which work as guides for the cables. The potential blockage due to the presence of steel posts is avoided in the RXI-100 with the insertion of runtop ropes, which bypass the post heads and base plates. External boundaries include fixing the translation of all the wire rope cables at the anchor points, where in the real assembly shackles connect the eyelets of wire ropes and ground bolts. For the ground plate, which is bolted to concrete foundations during installations, all the degrees of freedom are fixed.The impacting mass, whose magnitude is equal to 3200 kg, was modelled with a 3D discrete rigid part having the shape defined in EAD 340059-00-0106 (EOTA, 2018). The impactor mass and inertia properties were assigned to a reference point, appropriately defined in the block center of mass. The accurate reproduction of the block shape is needed to model contact interactions between the parts. Interaction properties were set using a general contact algorithm. The normal behaviour is modelled with a hard contact, while the tangential behaviour has a penalty contact. Coherently to existing studies in the field (Jin et al. 2021, Qi et al. 2023) the friction coefficient was set equal to 0.1 for steel to steel contact and to 0.4 for concrete to steel contact.

In the simulation, the Dynamic Explicit solutor was used. The simulation time was set to 0.6 s. After performing a mesh sensitivity analysis, the resulting stable time increment is in the order of 1·10-6 s. The net, which is the most critical element in terms of possible failures, is discretized with square shell elements with 50 mm side, while, due to the presence of connectors, 5 mm mesh was necessary for the beam elements. The impacting velocity (25 m/s) was assigned as a predefined field to the impactor reference point, as prescribed by the EAD for the execution of a MEL test. Four impact position were assigned, as reported in Fig. 2. Position 1 is in the center of the module, while the others are located in the sides.

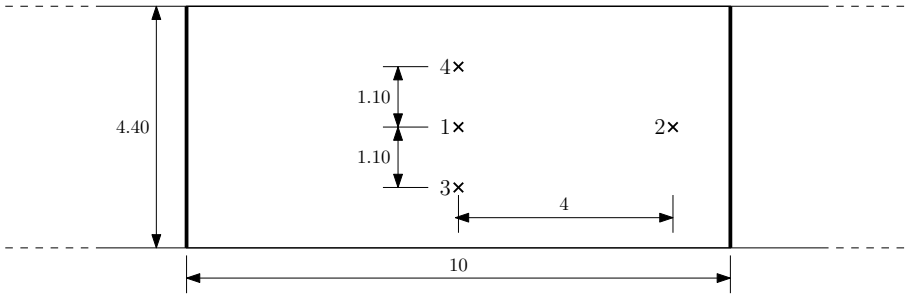

Fig. 2 Position of the simulated impacts in the central module (view from upslope).

3 Results

3.1 Centered impact

The present section describes the results obtained for a centered impactas prescribed by the EAD 340059-00-0106. The numerical time-history of the kinematics of the masses provides the deceleration force acting on the block. It results that the interaction force between the block and the net is the product of the mass of the block (3200 kg) and the opposite of the recorded acceleration. Fig. 3a depicts the time-history of the interaction force. It is seen that the impact starts at 61 ms and roughtly lasts 500 ms. After an initial plateau at 50 kN, a sudden increase occurs at around 220 ms. A higher plateau at 570 kN is then observed from 310 to 380 ms and the force peak occurs at 387 ms (660.6 kN). Block velocity decreases from 25 m/s and at 384 ms the mass is at rest, resulting that all the kinetic energy has been converted into elastic and plastic energies. Hence, the braking time is 384 – 61 = 323 ms. The force from 384 to 500 ms is the elastic restitution of the system which causes the rebound of the block. Fig. 3b reports the time-history of the integral of the force over time $\int_0^\tau Fdt$. The value corresponding to 600 ms (end) is the total impulse of the force. It is noted that the integral up to 384 ms (when the impacting mass is at rest) is equal to 80.4 kNs: from the impulse theorem, this value is equal to the variation of momentum of the mass, resulting that the initial velocity is 25.1 m/s and thusconfirming what previously considered. Such values are reported in Table 1.

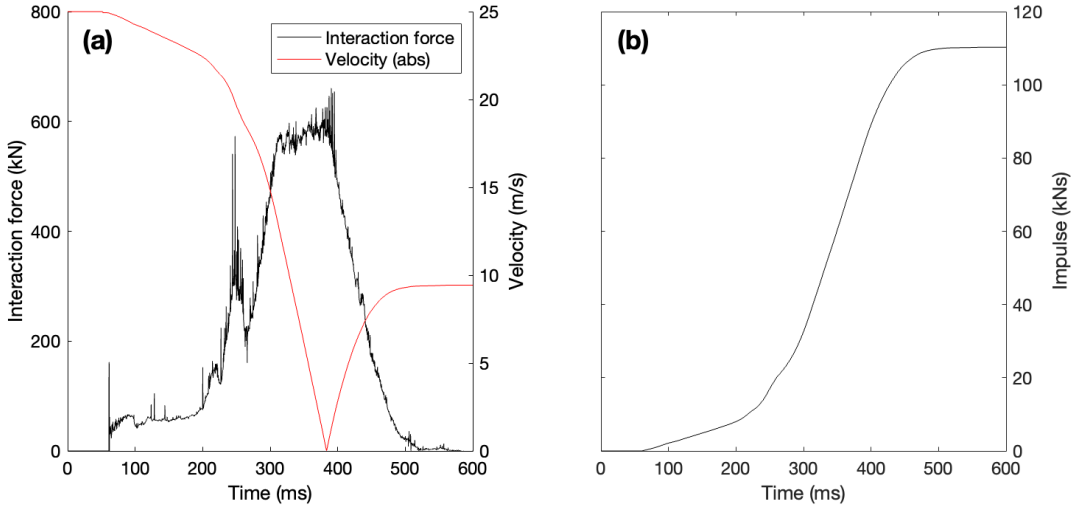

Fig. 3 Time-histories of (a) the interaction force and the absolute velocity of the block and (b) the values of $\int_0^\tau Fdt$ for the centered impact.

Fig. 4a reports the time-histories of the forces in the brakes, which are connected to the longitudinal ropes. It is seen that the activation of the brakes occurs at around 120 ms, i.e. 59 ms after the impact. This can be considered as the "response time" of the structure. The maximum forces are recorded when the mass is at rest and range from 162.5 and 186 kN. The stroke, i.e. the maximum elongation of the equivalent dissipator, is almost the same for all devices, with a minimum of 75 cm and a maximum of 96 cm (Table 2). Fig. 4b illustrates the time-histories of the forces in the upslope ropes. Some points have to be highlighted. First, the forces in the ropes are null up to 200 ms, i.e. 140 ms after the start of the block-net interaction. This is due to the fact that the intercepting net starts deforming without interacting with the supporting structure and connection components. As the impact is centered, the forces have the same trend in all the upslope ropes that are connected to the side posts of the central module as can be observed in Fig. 4b. Side ropes are activated, with a major contribution of S-Left and S-Right ropes (Fig. 4c). The maximum force in the ropes is reported in Table 3.

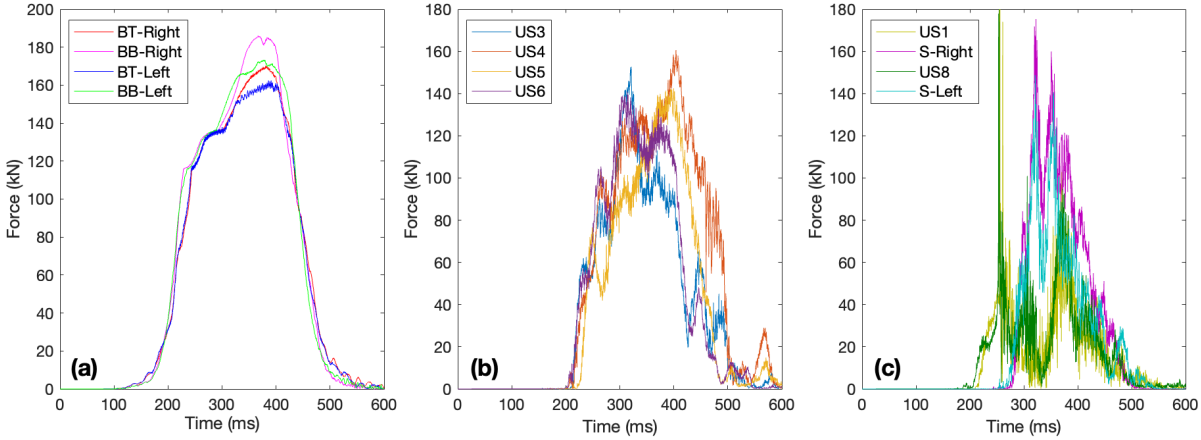

Fig. 4 Time-histories of forces in the upslope ropes (a) supporting the central posts and (b) the side posts. Refer to Fig. 1 for their position.

3.2 Non-centered impacts

The same calculations were repeated for non-centered impacts. Three additional cases have been examined, as depicted in Fig. 1. The comparison between the main recorded parameters is reported in Tables 1, 2 and 3. Observing the results related to the braking effects in Table 1, it is noted that there are no relevant differences on the forces exerted by the ring net to the block. A different behavior is noted comparing the forces and stroke on the brakes. In the centered case, as mentioned, the forces are almost the same across all the four devices. It is seen that when the impact occurs on the right side of the module, the balance of the forces and the dissipation is non trivial. Referring to the brakes, the larger strokes and forces are recorded in the left brakes, while the maximum forces are observed in the upslope ropes on the right side (i.e. close to the impact), in particular US4 (impact position 2 in Table 2 and 3), and a reduced elongation is observed in the net. Observing the other simulated cases, it is

interesting to note that a vertical eccentricity in the impact position (3 and 4) has different response on the system. For impact in position 3 (central-bottom), the bottom brakes of both ends experience larger force and larger stroke. Observing the time-history of the force, here not reported, it is found that the bottom longitudinal rope (and, hence, the dissipators at each end) is activated roughtly 100 ms before the top connector. Such a large difference in the response is not observed when the impact is in position 4 (central-top). From this preliminar results is thus possible to state that, in a risk mitigation design, an increase of the barrier height could not provide advantages in term of risk reduction.

Table 1 Braking effects on the block. The maximum braking force is maximum value of the product of the mass of the block (3200 kg) and the opposite of the recorded acceleration.

Impact position	Braking time (ms)	Maximum net elongation (m)	Impulse (kNs)	Maximum braking force (kN)	Mean braking force (kN)
1	323	6.69	80.4	660.6	248.9
2	295	5.94	79.8	644.1	271.2
3	311	6.32	79.9	711.3	256.9
4	325	6.46	79.9	590.1	245.8

Table 2 Maximum forces acting on the brakes and stroke (in square brackets).

Impact position	BT-Right (kN – m)	BB-Right (kN – m)	BT-Left (kN – m)	BB-Left (kN – m)
1	170.3 (0.82)	186.0 (0.96)	162.5 (0.75)	173.4 (0.85)
2	117.0 (0.10)	116.0 (0.09)	160.4 (0.71)	167.4 (0.80)
3	136.6 (0.43)	196.3 (1.03)	138.5 (0.51)	208.1 (1.13)
4	177.0 (0.87)	138.1 (0.53)	176.0 (0.86)	146.9 (0.62)

Table 3 Maximum force on the upslope ropes.

Impact position	US3 (kN)	US4 (kN)	US5 (kN)	US6 (kN)	US1 (kN)	S-Right (kN)	US8 (kN)	S-Left (kN)
1	152.7	160.7	142.5	141.0	178.2	175.3	191.0	148.7
2	162.4	253.3	86.6	67.4	97.0	116.6	65.6	219.1
3	157.9	114.5	108.2	182.3	102.1	171.1	88.1	216.2
4	150.4	170.0	198.2	168.1	80.0	127.9	63.3	119.0

Comparing the maximum force in the upslope ropes of Table 3, that are directly connected to the foundations without any dissipating device, it is interesting to note that when the impact is non centered (position 2) an unbalance of the forces is observed. Taking the centered impact (position 1) as a reference, it is noted that the eccentric impact along the width of the module causes a large increase (up to 50%) in the ropes connecting the closer post. A strongly asymmetrical stress in the retaining ropes in case of eccentric impact on the central module has been also observed in field tests conducted by WSL and reported in Caviezel et al. (2022) on a 60 m long barrier of Geobrugg AG with a MEL of 2000 kJ and 5 m high, with artificial blocks (EOTA 2018) rolling on a slope. Despite performed with other research purposes, also the field tests campaign on the same 2000 kJ product done by Geobrugg AG found that the forces in the retaining ropes are on average 20% higher during eccentric impact than in central ones with a maximum of 30%, while the absorption by the U-Brakes in both processes is approximately identical. These tests replicated the standardized tests as in EOTA 2018 but with eccentric impacts in the central module, similar to those investigated in the present study.

Summarizing, in the present analyses, no relevant changes are observed for eccentric impacts along the height of the module. For a given impacting energy and the studied product, blocks impacting in the lower lateral part of the barrier can produce the highest damage. Despite comparable, it is interesting observing how the results are product dependent: as an example, a similar campaign of numerical analyses has been conducted by Zhao et al. (2020) on a different product with a MEL of 2000 kJ. Also in this case, the inner side of the side region of the middle functional module reveals to be the most critical, while the peak forces of support ropes are not significantly influenced by impact positions due to buffering of energy dissipating devices, present in a different amount and in all the ropes.

3.3 A probability density to descrive the capacity E_b

The previous results represent a base to obtain a more reliable distribution of the capacity of a barrier. Despite simplified, a way to includ the obtained results into a simplified probabilistic model of the

capacity of the barrier is proposed. The same approach can thus be used with an extended campaign of analyses. The forces in the upslope ropes were considered as the relevant parameter to control the failure probability. In other words, it is expected that an impact that is eccentric along the width is more likely to cause the failure of the system as the forces in the upslope ropes are larger than in the centered case. Comparing impact positions 2 and 1, as highlighted, maximum forces larger than 50% are recorded when the impact energy is the same. This can be seen as block impacting at position 2 with reduced energy would generate forces in the upslope ropes similar to those at position 1 at barrier capacity. Based on the simple analyses, a capacity reduction reduction of 1/1.50 = 0.66 for impacts occurring in position 2 can be considered. Comparable barrier capacity in position 2 results can be achieved by calculating the increased brake stroke for eccentric impacts relative to the maximum allowable elongation and proportionally reducing the barrier capacity for centered impacts.

From these preliminary analyses, it can be proposed to subdivide a net fence central module in 7 areas, according to Fig. 5a: a 4 m wide central part, plus lateral parts. The central (light yellow) area (17.6 m^2) represents the 45% of the total surface of the module (44 m^2) and the barrier is considered able to resist the full capacity if an impact occurs there. The impact position 2 falls in the lateral (orange) area, which occupies a total of 8.8 m^2 representing the 20% of the surface of the module. The capacity of the barrier in case of an impact occurring in the lateral area is the 66% of the nominal capacity. A similar analysis can be performed for side central and far lateral areas for which the reductions of the capacity are 1/1.25=0.80 and 1/2=0.50, respectively.

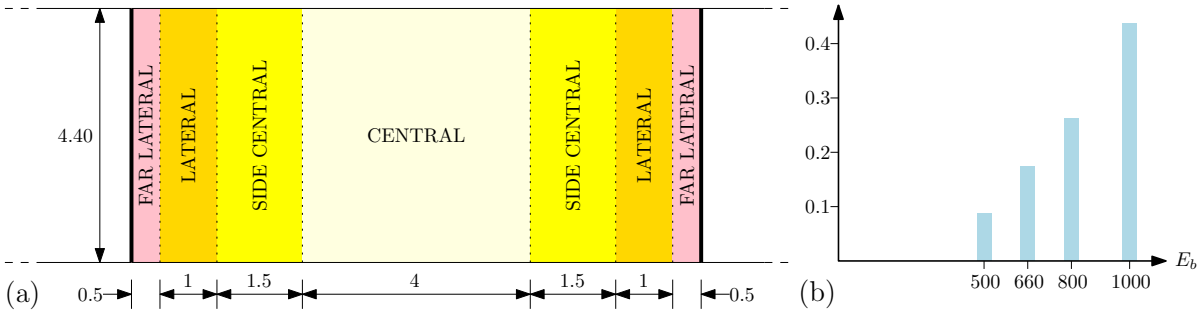

Fig. 5 The 10 m wide module is divided into 7 areas (a), and a tentative of discrete probability density (b).

Following the previous calculations, the capacity of the barrier is 1000 kJ if the impact occurs in the central area, 800 kJ in the side central area, 660 kJ in the lateral area, and 500 kJ in the far lateral area. The probability associated to each of the previous capacities is the ratio between the surface of each area and the total surface of the module, i.e., 0.45, 0.27, 0.18, and 0.10, respectively. This resuls in the discrete probability density depicted in Fig. 5b. Knowing the distributions of blocks velocities and masses, we can discretize in the same classes the distribution of possible impacting energies of Eq. (1) and, provided the knowledge of the probability associated to each class, check the failure probability of the system. Assuming, as an example, an impact with 70% of probability of an energy lower than 500 kJ, 15% between 500 and 660 kJ, 7% between 660 an 800 kJ, 5% between 800 and 1000 kJ, and 3% between 1000 and 1100 kJ, we obtain the probability of failure in case of an event. The integral of Eq. (1) results equal to: $1 - [1 \cdot 0.7 + (0.45 + 0.27 + 0.18) \cdot 0.15 + (0.45 + 0.27) \cdot 0.07 + 0.45 \cdot 0.05 + 0 \cdot 0.03] = 0.0921$, which is the failure probability when an event occurs. Consideringt Considering an average frequency of rockfall events of 0.067, i.e. an event every 15 years, the annual failure probability F_k results equal to $6.1 \cdot 10^{-3}$.

4 Conclusions

Rockfall protection structures are installed along the slopes to motigate the risk. As other structures, they are subjected to failure. Based on previous works by the Authors, the failure probability of the barrier, which capacity has been described with a Dirac-δ distribution at the nominal capacity, entrers in the reliability-based framework to quantify the effectiveness of the protection in the overall risk reduction. Based on the results of a numerical FEM modelling of a Geobrugg 1000 kJ barrier, an analysis on the position of the impact and the effects on the capacity is proposed. Although simplified, the approach is a further step for including the randomness of rockfall phenomenon into the design of mitigation measures and in risk quantification.

Acknowledgements

This paper was produced while (F.P.) attending the PhD programme in Civil and Environmental Engineering at Politecnico di Torino, cycle XXXVIII, with the support of a scholarship co- financed by the Ministerial Decree no. 352 of 9th April 2022, based on the NRRP - funded by the European Union - NextGenerationEU - Mission 4 “Education and Research”, Component 2 “From Research to Business”, Investment 3.3, and by the company Geobrugg AG.

References

Caviezel, A., Munch, J., Bartelt, P., & Lanter, A. (2022). Rockfall barrier service loads for rock impacts with spin. Theory and experiments. WSL Berichte: Vol. 125. 10.55419/wsl:32009

CEN (2002) EN 12385-4:2002 Steel wire ropes. Safety - Stranded ropes for general lifting applications. European Committee for Standardization, Brussels, Belgium.

De Biagi V, Marchelli M, Peila D (2020) Reliability analysis and partial safety factors approach for rockfall protection structures. Engineering Structures 213 100553. 10.1016/j.engstruct.2020.110553.

EOTA (2018) EAD 340059-00-0106 European Assessment Document: Falling Rock Protection Kits. European Organisation for Technical Assessment, Brussels, Belgium.

Escallón JP, Wendeler C, Chatzi E, Bartelt P (2014) Parameter identification of rockfall protection barrier components through an inverse formulation, Engineering Structures 77: 1-16. 10.1016/j.engstruct.2014.07.019

Forni D, Chiaia B, Cadoni E (2016) Strain rate behaviour in tension of S355 steel: Base for progressive collapse analysis. Engineering Structures 119: 164-173. 10.1016/j.engstruct.2016.04.013

Jin Y, Yu Z, Luo L, Guo L, Zhang L (2021) A membrane equivalent method to reproduce the macroscopic mechanical responses of steel wire-ring nets under rockfall impact. Thin-Walled Structures 167: 108227. 10.1016/j.tws.2021.108227

Marchelli M, De Biagi V, Peila D (2020) Reliability-Based Design of Protection Net Fences: Influence of Rockfall Uncertainties through a Statistical Analysis. Geosciences 10: 280. 10.3390/geosciences10080280

Marchelli M, De Biagi V, Peila D (2021) Reliability-based design of rockfall passive systems height. International Journal of Rock Mechanics and Mining Sciences 139: 104664. 10.1016/j.ijrmms.2021.104664

Marchelli M, De Biagi V, Chiaia B (2024) A fully probabilistic framework to compute the residual rockfall risk in presence of mitigation measures. Landslides: 8. 10.1007/s10346-024-02377-8.

Moos, C., Bontognali, Z., Dorren, L., Jaboyedoff, M., & Hantz, D. (2022). Estimating rockfall and block volume scenarios based on a straightforward rockfall frequency model. Engineering Geology, 309, 106828. 10.1016/j.enggeo.2022.106828

Pimpinella F, Marchelli M, De Biagi V (2024) A weight-based efficiency measure for energy dissipating devices for flexible rockfall barriers. International Journal of Protective Structures: 25. 10.1177/20414196241299126

Qi X, Xu H, Yu Z, Zhao L, Meng Q (2018) Dynamic mechanical property study of break rings in flexible protective system, Engineering Mechanics 35 (9): 188-196. 10.6052/j.issn.1000-4750.2017.06.0438

Qi X, Deng Q, Zhao L, Yuan S, Li Z, Wang X, Yu Z (2023) Equivalent relationship of the mechanical behavior of ring nets under static punching and dynamic impact conditions, Buildings 13(3): 588. 10.3390/buildings13030588

Ribeiro J, Santiago A, Rigueiro C (2016) Damage model calibration and application for S355 steel. Procedia Structural Integrity 2: 656-663. 10.1016/j.prostr.2016.06.085

UNI (2018) UNI 11211-4: 2018 Rockfall protective measures. Part 4: Definitive and executive design. UNI Ente Nazionale Italiano di Unificazione, Milano, Italy.

Xu H, Gentilini C, Yu Z, Qi Z, Zhao S (2018) An energy allocation based design approach for flexible rockfall protection barriers. Engineering Structures 173: 831-852.1016/j.engstruct.2018.07.018

Zhao, L., Yu, Z. X., Liu, Y. P., He, J. W., Chan, S. L., & Zhao, S. C. (2020). Numerical simulation of responses of flexible rockfall barriers under impact loading at different positions. Journal of Constructional Steel Research, 167, 105953. 10.1016/j.jcsr.2020.105953